Liquid is More Rigid than Solid in a High-Frequency Region: *Supplemental Material*

Naoki Hasegawa,[1] Tatsuro Yuge,[2,*] and Akira Shimizu[1,†]

[1] *Department of Basic Science, University of Tokyo, 3-8-1 Komaba, Meguro, Tokyo 153-8902, Japan*
[2] *Department of Physics, Osaka University, 1-1, Toyonaka, Osaka, 560-0043, Japan*

(Dated: November 16, 2015)

We present details of our model for the MD simulation, dependence of the admittance on the configuration of impurities (pinning centers), that on the system size, and derivation of the restricted sum rule for the longitudinal admittance.

I. DETAILS OF THE MODEL FOR NONEQUILIBRIUM MD SIMULATION

We first present details of our model for the MD simulation. More details are described in Ref. [1].

As shown in Fig. 1 of the paper, our model consists of three types of particles, which are called e, p and i after a typical case where they are electrons, phonons and impurities, respectively. Their numbers are N_e, N_p and N_i, respectively. We impose periodic boundary conditions of size $L_x \times L_y \times L_z$. The Hamiltonian is given by

$$H = K_e + K_p + V_{ee} + V_{ep} + V_{ei}, \tag{S.1}$$

where K_e and K_p are kinetic energies of e and p particles, respectively, whereas V_{ee}, V_{ep} and V_{ei} are e-e, e-p and e-i interactions, respectively.

For $V_{\alpha\beta}$ $(\alpha, \beta = e, p, i)$, we take the following short-range interactions;

$$V_{\alpha\beta} = U \sum_{j=1}^{N_\alpha} \sum_{l=1}^{N_\beta} \left(R_\alpha + R_\beta - |\boldsymbol{q}_\alpha^j - \boldsymbol{q}_\beta^l|\right)^3 \tag{S.2}$$

for $R_\alpha + R_\beta - |\boldsymbol{q}_\alpha^j - \boldsymbol{q}_\beta^l| \geq 0$, whereas $V_{\alpha\beta} = 0$ otherwise, where $\boldsymbol{q}_\alpha^j$ and $\boldsymbol{q}_\beta^l$ are positions of the j-th α and the l-th β particles, respectively. Here, U, R_α and R_β are positive constants, representing the strength of the interaction, the radiuses of α and β particles, respectively.

U is taken very large $(= 10000)$, so that $V_{\alpha\beta}$'s are close to hard-core interactions. We take $R_e = 1$, whereas $R_p = R_i = 0$ (hence interactions between p and i particles are absent). Hence, with increasing the volume filling factor $\rho_e = (4\pi/3)N_e/(L_x L_y L_z)$, e particles undergo a first-order transition of the Alder type [2, 3], from a liquid phase ($\rho_e < \rho_e^{\rm lq}$) to a solid phase ($\rho_e > \rho_e^{\rm sl}$). Both phases coexist for $\rho_e^{\rm lq} \leq \rho_e \leq \rho_e^{\rm sl}$. For hard-sphere particles of unit radius, $\rho_e^{\rm lq} = 0.494$ and $\rho_e^{\rm sl} = 0.545$ [3]. By contrast, neither p nor i particles undergo such a transition because they have vanishing volume densities (because $R_p = R_i = 0$). Note that temperature is irrelevant for hard-sphere particles because changing temperature is equivalent to changing the time scale, and hence the transition point is independent of temperature [2, 3].

The p particles are particles of the 'environment,' which is attached to a heat reservoir. Through e-p interaction p particles tend to drive the temperature of e particles to that of the reservoir, T. The i particles are 'impurities,' which are fixed at random positions, and scatter e particles via static potentials. They work as pinning centers. For the mass of e and p particles, we take $m_e = m_p = 1$.

A force $\boldsymbol{f}(t)$ acts only on e particles. Work done by $\boldsymbol{f}(t)$ on e particles is distributed among e and p particles, through the e-e and e-p interactions, and finally dissipated to the reservoir. As a result, a stable nonequilibrium state is realized in the presence of $\boldsymbol{f}(t)$, and the system has well-defined $\Xi(\omega)$.

The heat reservoir attached to p particles was modeled in the previous works [4–8] by thermal walls. However, such a model is not appropriate for the present purpose because, when $\boldsymbol{f} \neq 0$, it induces inhomogeneity of temperature, which will obscure a phase transition. We therefore employ another reservoir model, in which thermal walls are effectively distributed uniformly in the system. Let

$$\tau_e \equiv \frac{L_x L_y L_z}{(N_e + N_p + N_i)\pi R_e^2} \sqrt{\frac{m_e}{2\pi k_{\rm B} T}}, \tag{S.3}$$

which is a time scale of the order of the mean scattering time of an e particle. In every $\tau_e/(2N_p)$ we choose randomly one of p particles, which are not in contact with e particles. We then reset the velocity of the chosen p particle to a random value that is taken from the Maxwell distribution. This tends to drive p particles to the thermal equilibrium of temperature T (we take $T = k_{\rm B} = 1$). On the other hand, thermal equilibrium among e particles are established (when $\boldsymbol{f} = 0$) by e-e interaction V_{ee}, and its temperature is driven to T through the e-p interaction V_{ep}.

We perform a time-step-driven MD on this model. We use Gear's fifth-order predictor-corrector method for the time integration of the Newton equations of particles. The initial configurations of the particles are prepared randomly in the liquid phase. In the solid phase, we first place e particles at the lattice points of the crystal structure. We then distribute p and i particles randomly in vacant spaces. We then let the system evolve without $\boldsymbol{f}(t)$ until a macroscopic steady (equilibrium) state is realized. We have taken this final state as the initial state in the solid phase.

* yuge@acty.phys.sci.osaka-u.ac.jp
† shmz@ASone.c.u-tokyo.ac.jp; http://as2.c.u-tokyo.ac.jp

We have confirmed that this model works well, in various ways [1]. When $\boldsymbol{f} = 0$, the system relaxes to equilibrium states quickly for all the initial states that we have tested. For example, when we give a large velocity $\boldsymbol{v} = (2, 0, 0)$ to all e particles at $t = 0$, their center-of-mass velocity relaxes quickly enough (relaxation time < 10), as shown in Fig. S1. Long after the relaxation time, the velocity distribution of e particles are well fitted by the Maxwell distribution, as shown in the right inset of Fig. S1. When $\boldsymbol{f} \neq 0$, this model has stable nonequilibrium states [1] like the previous models [4–8]. These good properties enable us to obtain reliable values of $\Xi(\omega)$, both for liquid and solid phases. We therefore expect that this model will be useful to explore various properties of equilibrium and nonequilibrium states. When computing the integral value of $\Xi'(\omega)$, we have set the upper bound of the integral to $\omega = 10$, above which $\Xi'(\omega)$ is vanishingly small (and hence relative errors are large). The simulation time is taken as $\max\{400\pi/\omega, 20000\}$, whereas the time step Δt is taken as 10^{-4}. We take $N_e = 320, N_p = 160, N_i =$ 0-80.

II. DEPENDENCE OF THE ADMITTANCE ON THE IMPURITY CONFIGURATION

We have shown in the main text that in a solid phase $\Xi'(\omega)$ has a peak at a high frequency, which makes the solid more flexible than the liquid. We here study the dependence of the peak on the configuration (spatial distributions) of impurities.

In Fig. S2, we plot $\Xi'(\omega)$ for various configurations of impurities, at the same concentration $N_i = 80$ of impurities, for the solid phase. To show variations of $\Xi'(\omega)$ clearly, we use linear scales for both the horizontal and vertical axes. (By contrast, we have used a logarithmic scale for the horizontal axis of Fig. 2 of the main text.) We observe that the peak position shifts slightly by $\sim \pm 0.1$. This indicates that the peak is not intrinsic to the e-particle solid.

However, as discussed in the main text, this point is seen more clearly by changing concentration N_i of impurities. To show this, we also plot $\Xi'(\omega)$ at another concentration $N_i = 40$ in Fig. S2. It is seen that the shift of the peak is larger than the case of changing configurations. For more discussions on the N_i dependence, see the main text.

III. DEPENDENCE OF THE ADMITTANCE ON THE SIZE

In the MD simulations of Figs. 2 and 3 of the paper, we have taken $N_e = 320, N_p = 160, N_i = 80$ and $(L_x, L_y, L_z) = (15, 12, 12)$ for the solid phase. To confirm that the finite-size effects are irrelevant, we have performed the simulations for a larger system size (which is 2.25 times larger in volume) with $N_e = 720, N_p = 360, N_i = 180$ and $(L_x, L_y, L_z) = (18, 18, 15)$.

The result for this larger system is plotted in Fig. S3 together with the one for the smaller system (i.e., the corresponding result which is shown in Fig. 2 of the paper). The difference between the results for the larger and smaller systems consists of the following contributions: (a) finite-size effects and (b) dependence on the impurity configurations (because the configurations of the impurities of the larger system are taken independently of those of the smaller system). The latter is already studied in Sec. II and Fig. S2 for the smaller system, and found to be weaker than the dependence on the impurity density. It is seen that the difference between the results for the larger and smaller systems, shown in Fig. S3, is the same order as the dependence on the impurity configurations, shown in Fig. S2. Therefore, contribution (a) $\lesssim$ contribution (b) $<$ dependence on the impurity density. This supports that the finite-size effects are irrelevant to the main conclusion.

IV. DERIVATION OF THE RESTRICTED SUM RULE FOR LONGITUDINAL ADMITTANCE

For completeness, we derive Eq. (5) in the main text, in a way similar to derivation of the restricted sum rule for the optical (transverse) conductivity [9–14].

Actually, we here derive a result more general than Eq. (5), i.e., we derive the restricted sum rule for longitudinal *differential* admittance of a *nonequilibrium* state that is driven by pump fields. By taking the limit of vanishing pump fields, the general result reduces to Eq. (5).

The setup of the system is almost the same as that in Ref. [14]. Suppose that a many-electron system is subject to two types of fields; one is a longitudinal electric field, described by a scalar potential $\phi(\boldsymbol{r}, t)$, and the other is an optical field, described by a vector potential $\boldsymbol{A}(t)$ (in the Coulomb gauge). These fields induce electrical conduction and optical excitation to make the system in a nonequilibrium state. We therefore call $A \equiv (\phi, \boldsymbol{A})$ pump field. It can be arbitrarily strong and have arbitrary time dependence.

To obtain the longitudinal response function of the nonequilibrium state, we apply another longitudinal field, described by a scalar potential $\varphi(\boldsymbol{r}, t) = -\boldsymbol{f}(t) \cdot \boldsymbol{r}$. We call $\boldsymbol{f}$ a probe (electric) field. We are interested in the φ-induced change in the electrical current $\boldsymbol{I}$: $\Delta\boldsymbol{I}(t) = \mathrm{Tr}[\hat{\rho}^{A+\varphi}(t)\hat{\boldsymbol{I}}] - \mathrm{Tr}[\hat{\rho}^{A}(t)\hat{\boldsymbol{I}}]$, where $\hat{\rho}^{A+\varphi}(t)$ and $\hat{\rho}^{A}(t)$ are the density matrices of the nonequilibrium states with and without the probe field, respectively. When $|\boldsymbol{f}|$ is sufficiently small, $\boldsymbol{f}(t)$ and $\Delta\boldsymbol{I}(t)$ are related as

$$\Delta I_\alpha(t) = \sum_\beta \int_{-\infty}^{t} dt' \Phi^A_{\alpha\beta}(t - t'; t) f_\beta(t'), \tag{S.4}$$

where $\alpha, \beta = x, y, z$. This equation and the causality, $\Phi^A_{\alpha\beta}(\tau < 0; t) = 0$, define the differential longitudinal conductivity tensor $\Phi^A_{\alpha\beta}$.

When $\boldsymbol{f}(t)$ is monochromatic, i.e., when $\boldsymbol{f}(t) = \boldsymbol{f}e^{-i\omega t} + \text{c.c.}$, Eq. (S.4) reads

$$\Delta I_\alpha(t) = \sum_\beta \Xi^A_{\alpha\beta}(\omega;t) f_\beta e^{-i\omega t} + \text{c.c.} \tag{S.5}$$

Here $\Xi^A_{\alpha\beta}(\omega;t)$ is the Fourier transform of $\Phi^A_{\alpha\beta}(\tau;t)$ with respect to τ and is called differential longitudinal admittance.

To connect the above argument with a microscopic theory, we consider a general model of the many-electron system that is restricted to a single band. The electrons move on a arbitrary regular lattice. The Hamiltonian of the model in the absence of A and φ is given by

$$\hat{H}_0 = \hat{H}_\text{e} + \hat{H}_\text{ei} + \hat{H}_\text{ee} + \hat{H}_\text{ep} + \hat{H}_\text{p}. \tag{S.6}$$

Here, $\hat{H}_\text{e}$ is the kinetic energy of electrons, $\hat{H}_\text{ei}$ is random potential produced by impurities, $\hat{H}_\text{ee}$ is the electron-electron interaction, $\hat{H}_\text{ep}$ is the electron-phonon interaction, and $\hat{H}_\text{p}$ is the Hamiltonian for free phonons. The kinetic energy of electrons is given by

$$\hat{H}_\text{e} = \sum_{\boldsymbol{l},\boldsymbol{l}',\sigma} t_{\boldsymbol{l}-\boldsymbol{l}'} \hat{c}^\dagger_{\boldsymbol{l}\sigma} \hat{c}_{\boldsymbol{l}'\sigma} + \text{h.c.} \tag{S.7}$$

$$= \sum_{\boldsymbol{k},\sigma} \varepsilon(\boldsymbol{k}) \hat{n}_{\boldsymbol{k}\sigma}. \tag{S.8}$$

Here, $t_{\boldsymbol{l}-\boldsymbol{l}'}$ is the transfer amplitude between sites $\boldsymbol{l}$ and $\boldsymbol{l}'$ (it depends only on the relative vector $\boldsymbol{l}-\boldsymbol{l}'$), $\hat{c}_{\boldsymbol{l}\sigma}$ is the electron annihilation operator on site $\boldsymbol{l}$ with spin σ, $\varepsilon(\boldsymbol{k})$ is the energy dispersion of the band of interest, and $\hat{n}_{\boldsymbol{k}\sigma} = \hat{c}^\dagger_{\boldsymbol{k}\sigma}\hat{c}_{\boldsymbol{k}\sigma}$, where

$$\hat{c}_{\boldsymbol{k}\sigma} = \frac{1}{\sqrt{N}} \sum_{\boldsymbol{l}} e^{i\boldsymbol{k}\cdot\boldsymbol{l}} \hat{c}_{\boldsymbol{l}\sigma}, \tag{S.9}$$

$$\varepsilon(\boldsymbol{k}) = \sum_{\boldsymbol{R}} t_{\boldsymbol{R}} e^{i\boldsymbol{k}\cdot\boldsymbol{R}} + \text{c.c.} \tag{S.10}$$

The concrete forms of the other terms in the Hamiltonian in Eq. (S.6) are not relevant to the subsequent argument.

We can incorporate the interaction with $\boldsymbol{A}$ by the Peierls substitution, and the interaction with ϕ and φ by the Coulomb interaction. Hence, the Hamiltonian in the presence of A and φ is given by

$$\hat{H} = \hat{H}^{\boldsymbol{A}}_\text{e} + \hat{H}^{\phi}_\text{e} + \hat{H}^{\varphi}_\text{e} + \hat{H}_\text{ei} + \hat{H}_\text{ee} + \hat{H}_\text{ep} + \hat{H}_\text{p}. \tag{S.11}$$

Here,

$$\hat{H}^{\boldsymbol{A}}_\text{e} = \sum_{\boldsymbol{k},\sigma} \varepsilon\big(\boldsymbol{k} - e\boldsymbol{A}(t)/\hbar\big)\hat{n}_{\boldsymbol{k}\sigma}$$

$$= \sum_{\boldsymbol{l},\boldsymbol{l}',\sigma} t_{\boldsymbol{l}-\boldsymbol{l}'} e^{-ie\boldsymbol{A}(t)\cdot(\boldsymbol{l}-\boldsymbol{l}')/\hbar} \hat{c}^\dagger_{\boldsymbol{l}\sigma}\hat{c}_{\boldsymbol{l}'\sigma} + \text{h.c.}, \tag{S.12}$$

$$\hat{H}^{\phi}_\text{e} = e\sum_{\boldsymbol{l}} \Big(\sum_\sigma \hat{c}^\dagger_{\boldsymbol{l}\sigma}\hat{c}_{\boldsymbol{l}\sigma} - n^\text{bg}_{\boldsymbol{l}}\Big)\phi(\boldsymbol{l},t), \tag{S.13}$$

$$\hat{H}^{\varphi}_\text{e} = e\sum_{\boldsymbol{l}} \Big(\sum_\sigma \hat{c}^\dagger_{\boldsymbol{l}\sigma}\hat{c}_{\boldsymbol{l}\sigma} - n^\text{bg}_{\boldsymbol{l}}\Big)\varphi(\boldsymbol{l},t)$$

$$= -\hat{\boldsymbol{D}}\cdot\boldsymbol{f}(t), \tag{S.14}$$

where e is the electron charge, $-en^\text{bg}_{\boldsymbol{l}}$ is a background charge on site $\boldsymbol{l}$, and

$$\hat{\boldsymbol{D}} = e\sum_{\boldsymbol{l}} \big(\sum_\sigma \hat{c}^\dagger_{\boldsymbol{l}\sigma}\hat{c}_{\boldsymbol{l}\sigma} - n^\text{bg}_{\boldsymbol{l}}\big)\boldsymbol{l}. \tag{S.15}$$

We obtain the electric current operator $\hat{\boldsymbol{I}}$ by differentiating $\hat{H}$ with respect to $\boldsymbol{A}$:

$$\hat{I}_\alpha = \frac{e}{L_\alpha}\sum_{\boldsymbol{k},\sigma} v_\alpha\big(\boldsymbol{k} - e\boldsymbol{A}(t)/\hbar\big)\hat{n}_{\boldsymbol{k}\sigma}$$

$$= \frac{e}{L_\alpha}\sum_{\boldsymbol{l},\boldsymbol{l}',\sigma} \frac{1}{i\hbar}(l_\alpha - l'_\alpha) t_{\boldsymbol{l}-\boldsymbol{l}'} e^{-ie\boldsymbol{A}(t)\cdot(\boldsymbol{l}-\boldsymbol{l}')/\hbar} \hat{c}^\dagger_{\boldsymbol{l}\sigma}\hat{c}_{\boldsymbol{l}'\sigma}$$

$$+\text{h.c.}, \tag{S.16}$$

where L_α is the system size in the α direction, and

$$v_\alpha(\boldsymbol{k}) \equiv \frac{1}{\hbar}\frac{\partial}{\partial k_\alpha}\varepsilon(\boldsymbol{k}) \tag{S.17}$$

is the velocity vector.

Then, regarding $\hat{\boldsymbol{I}}$ as the observable of interest and $\hat{H}^{\varphi}_\text{e}$ as the probe Hamiltonian, we use the result [Eq. (13)] in Ref. [15] to obtain the sum rule:

$$\int_{-\infty}^{\infty} \text{Re}\Xi^A_{\alpha\beta}(\omega;t)\frac{d\omega}{\pi} = \frac{1}{i\hbar}\text{Tr}\left\{\hat{\rho}^A(t)[\hat{D}_\beta, \hat{I}_\alpha]\right\} \tag{S.18}$$

By substituting Eqs. (S.15) and (S.16) into the above equation and by straightforward calculation, we get

$$\int_{-\infty}^{\infty} \text{Re}\Xi^A_{\alpha\beta}(\omega;t)\frac{d\omega}{\pi}$$

$$= -\frac{e^2}{L_\alpha\hbar^2}\sum_{\boldsymbol{l},\boldsymbol{l}',\sigma}(l_\alpha - l'_\alpha)(l_\beta - l'_\beta)$$

$$\times\text{Tr}\left\{\hat{\rho}^A(t)\big(t_{\boldsymbol{l}-\boldsymbol{l}'}e^{-ie\boldsymbol{A}(t)\cdot(\boldsymbol{l}-\boldsymbol{l}')/\hbar}\hat{c}^\dagger_{\boldsymbol{l}\sigma}\hat{c}_{\boldsymbol{l}'\sigma} + \text{h.c.}\big)\right\}.$$

Furthermore, using Eqs. (S.9) and (S.10), we finally obtain the general result for the restricted sum rule for the longitudinal admittance as

$$\int_{-\infty}^{\infty} \text{Re}\Xi^A_{\alpha\beta}(\omega;t)\frac{d\omega}{\pi}$$

$$= \frac{e^2}{L_\alpha} m^{-1}_{\alpha\beta}\big(\boldsymbol{k} - e\boldsymbol{A}(t)/\hbar\big)\text{Tr}\left\{\hat{\rho}^A(t)\hat{n}_{\boldsymbol{k}\sigma}\right\}. \tag{S.19}$$

Here,

$$m^{-1}_{\alpha\beta}(\boldsymbol{k}) \equiv \frac{1}{\hbar^2}\frac{\partial^2}{\partial k_\alpha \partial k_\beta}\varepsilon(\boldsymbol{k}) \tag{S.20}$$

is the inverse mass tensor.

By taking $\alpha = \beta = x$ and setting $\boldsymbol{A} = 0$ and $\phi = 0$, we obtain Eq. (5) in the main text as a special case of the general result (S.19).

[1] N. Hasegawa, Master Thesis (University of Tokyo, 2014).
[2] B. J. Alder and T. E. Wainwright, J. Chem. Phys. **27**, 1208 (1957).
[3] W. G. Hoover and F. H. Ree, J. Chem. Phys. **49**, 3609 (1968).
[4] T. Yuge, N. Ito and A. Shimizu, J. Phys. Soc. Jpn. **74**, 1895 (2005).
[5] T. Yuge and A. Shimizu, J. Phys. Soc. Jpn. **76**, 093001 (2007); *Erratum:* J. Phys. Soc. Jpn. **77**, 028001 (2008).
[6] T. Yuge and A. Shimizu, Prog. Theor. Phys. Suppl. **178**, 64 (2009).
[7] T. Yuge and A. Shimizu, J. Phys. Soc. Jpn. **78**, 083001 (2009).
[8] F. Lee, T. Yuge and A. Shimizu, J. Phys. Soc. Jpn. **81** 064710 (2012).
[9] P. C. Martin: Phys. Rev. **161** (1967) 143.
[10] S. Chakravarty: Eur. Phys. J. B **5** (1998) 337.
[11] L. Benfatto, S. G. Sharapov, N. Andrenacci, and H. Beck: Phys. Rev. B **71** (2005) 104511.
[12] D. N. Basov and T. Timusk: Rev. Mod. Phys. **77** (2005) 721.
[13] V. Vescoli, J. Favand, F. Mila, and L. Degiorgi: Eur. Phys. J. B **3** (1998) 149.
[14] A. Shimizu and T. Yuge, J. Phys. Soc. Jpn. **80**, 093706 (2011).
[15] A. Shimizu and T. Yuge, J. Phys. Soc. Jpn. **79**, 013002 (2010).

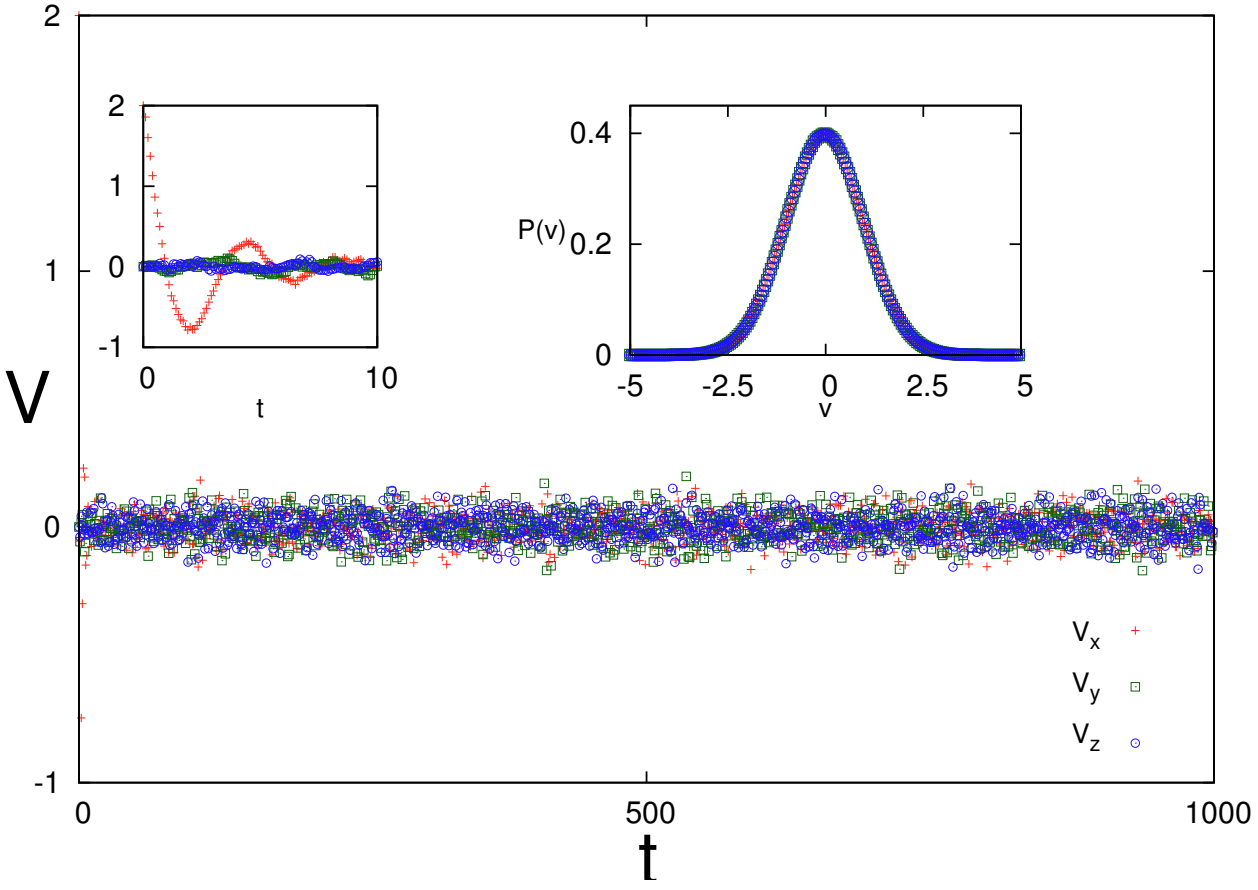

FIG. S1. Velocity $\boldsymbol{V} = (V_x, V_y, V_z)$ of the center-of-mass of e particles, for which we let $\boldsymbol{v}(0) = (2, 0, 0)$ for all e particles, is plotted as a function of time. For clarity of the plot, we plot $\boldsymbol{V}(t)$ at $t = 10000n\Delta t$ $(n = 0, 1, 2, \cdots)$, where Δt is the time step of the MD simulations (we take $\Delta t = 10^{-4}$). (Left inset) Magnification of this plot in an early time stage. (Right inset) Velocity distribution of e particles for $1000 \leq t \leq 2000$, where the Maxwell distribution is denoted by the red solid curve.

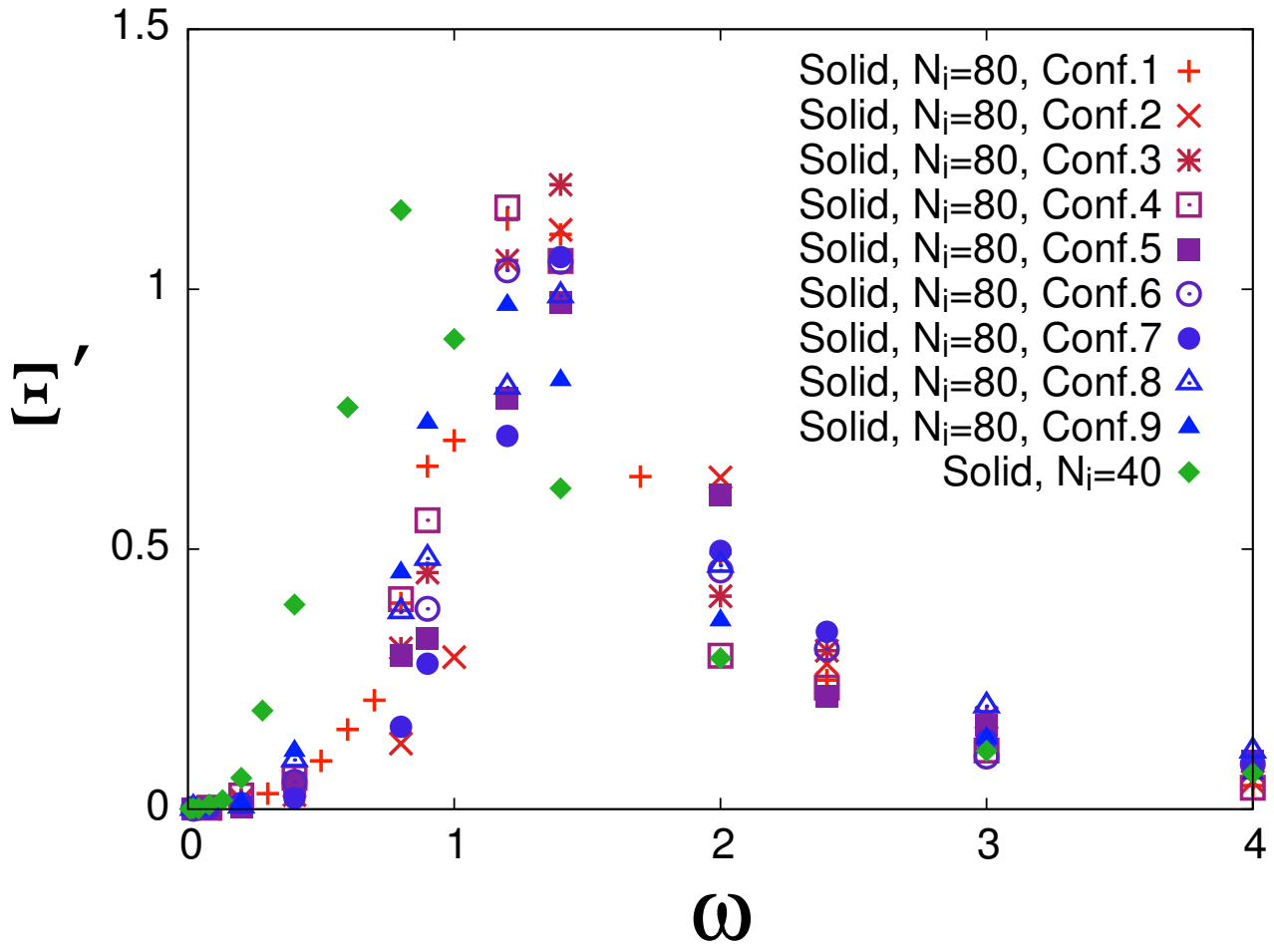

FIG. S2. The real part $\Xi'(\omega)$ of the admittance for various configurations of impurities, at the same concentration $N_i = 80$ of impurities, for the solid phase with $(L_x, L_y, L_z) = (15, 12, 12)$, $N_e = 320, N_p = 160$ and $T = 1$. For comparison, $\Xi'(\omega)$ at another concentration $N_i = 40$ of impurities is also shown.

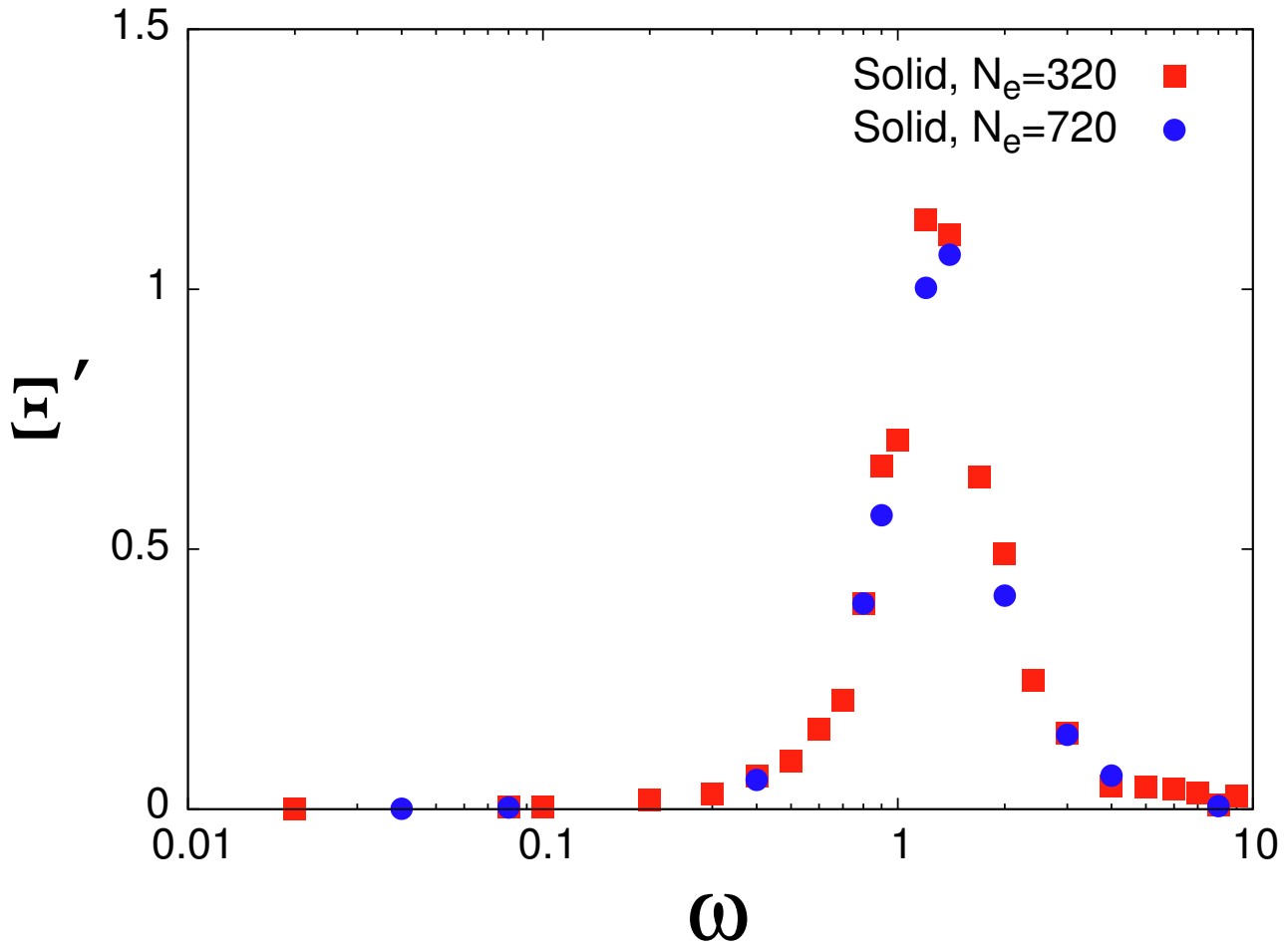

FIG. S3. The real part $\Xi'(\omega)$ of the admittance for the solid phase, with $N_e = 720, N_p = 360, N_i = 180, (L_x, L_y, L_z) = (18, 18, 15)$ (blue circle), and with $N_e = 320, N_p = 160, N_i = 80, (L_x, L_y, L_z) = (15, 12, 12)$ (red square).